Biophysical Journal, Volume *113*

Supplemental Information

Dynamic Scaling Analysis of Molecular Motion within the LAT:Grb2:-SOS Protein Network on Membranes

William Y.C. Huang, Han-Kuei Chiang, and Jay T. Groves

Supporting Materials and Methods

Experimental methods and materials used in this study were similar to previous studies (1).

Chemicals

1,2-dioleoyl-sn-glycero-3-phosphocholine (DOPC) and 1,2-dioleoyl-sn-glycero-3-[(N-(5-amino-1-carboxypentyl)iminodiacetic acid)succinyl] (nickel salt) (Ni^{2+}-NTA-DOGS) were purchased from Avanti Polar Lipids. Texas Red 1,2-dihexadecanoylsn-glycero-3-phosphoethanolamine (TR-DHPE) was purchased from Invitrogen. Alexa Fluor 647 maleimide dye and Alexa Fluor 561 maleimide dye were purchased from Life Technology. Bovine Serum Albumin (BSA), (±)-6-Hydroxy-2,5,7,8-tetramethylchromane-2-carboxylic acid (Trolox), Catalase, 2-Mercaptoethanol (BME), $NiCl_2$, H_2SO_4 and ATP were purchased from Sigma-Aldrich. Glucose Oxidase was purchased from Serva. Tris(2-carboxyethyl)phosphine (TCEP) was brought from Thermo Scientific. Glucose and H_2O_2 were from Fisher Scientific. $MgCl_2$ was from EMD Chemicals. Tris buffer saline (TBS) was purchased from Corning.

Protein Purification

LAT, Grb2 and SOS1 are purified similarly to previously work (1, 2). Human LAT cytosolic domain (residues 30 to 233) and full-length Grb2 were purified as described previously (2) using an N-terminal 6-His tag, while proline rich domain of SOS (residue 1051-1333) was purified with similar strategy (1). For both Grb2 and SOS, the N-terminal 6-His tag were removed with Tobacco Etch Virus protease. LAT, Grb2 and SOS were labeled with Alexa Fluor 555, Alexa Fluor 647, Alexa Fluor 647, respectively, using maleimide-thiol chemistry for fluorescently labeled construct.

Protein labeling using maleimide

LAT, Grb2 or SOS were diluted to 100 μM (or less). The proteins were then allowed to react with 1 mM Alexa Fluor 561 or 647 maleimide dye for 2 hrs at room temperature. The reaction was then quenched with 5 mM BME for 10 min. Excess dye was removed by size exclusion chromatography (Superdex 75 (LAT) or Sephadex G-25 (Grb2)).

Functionalized Supported Membranes

Glass substrates (no. 1.5 thickness) were prepared by 5 min piranha etching (H_2SO_4:H_2O_2 = 3:1 by volume), followed by excessive rinsing of H_2O (Milli-Q). Glass substrates were blow dried with air before depositing vesicles to form supported lipid bilayers (SLBs). Small unilamellar vesicles (SUVs) were prepared by mixing DOPC: Ni^{2+}-NTA-DOGS = 96:4 by molar percent in chloroform. If visualization of the bilayers was required, additional 0.005% of TR-DHPE was added to the lipid composition. The solution mixture was then evaporated by a rotary evaporator for 15 min at 40°C. Lipid dried films were further dried with N_2 for another 15 min. The lipids were resuspended in H_2O by vortexing, resulting in a concentration of ~0.5 mg/mL. Finally, the vesicle solution was sonicated with a sonicator for 90 s in an ice-water bath. The membrane system was prepared on a flow chamber (μ-Slid, Ibidi). SLBs were formed on a glass substrate by incubating the SUVs mixed with 40 mM TBS for at least 30 min. The chambers were rinsed with TBS buffer. TBS buffer refers to 20 mM TBS buffer with 5mM $MgCl_2$ at pH 7.4 unless stated otherwise. Next, 1 mg/mL BSA in TBS buffer was incubated for 10 min to block defects in supported membranes. Before protein incubation, the system was buffer exchanged into TBS buffer containing 1 mM TCEP. Proteins were centrifuged for 20 min at 4°C beforehand to remove possible aggregates. Hck and LAT were incubated at 31 and 126 nM, respectively, for 10 min to attach to the bilayers via his-tag Ni^{2+}NTA chemistry (3). The system was allowed to sit for another 20 min to allow unstably bound membrane proteins to dissociate from the surface.

Between all incubation steps, the chambers were rinsed with TBS buffer. Fluidity of the membrane-bound proteins was examined by fluorescent recovery after photobleaching (FRAP). Densities of membrane proteins were estimated by establishing a calibration curve between epifluorescence average intensity and densities measured by fluorescence correlation spectroscopy (FCS) (FCS methods were described previously (4)). LAT assembly was formed by addition of 5.8 μM Grb2, 1.45 μM proline-rich domain of SOS, and 1 mM ATP in scavenger buffer (2 mM UV-treated trolox, 10 mM BME, 20 mM glucose, 320 μg/mL glucose oxidase, 50μg/mL catalase (5)). All parts of preparation were done at room temperature unless otherwise stated.

Single-molecule imaging

Total internal reflection microscopy (TIRF) configuration was setup on a Nikon Eclipse Ti inverted microscopy. TIRF excitations were performed with 561 nm (Sapphire HP, Coherent Inc) laser lines. The optical path was then aligned to a 100x 1.49 NA oil immersion TIRF objective (Nikon). The excitation filter was done with a customized filter optimized for 561 nm (Semrock). The emission was further filtered with 630/75 nm bandpass filter (ET630/75M)). An Andor iXon EMCCD camera was used to record the signals. MetaMorph software (Molecular Devices Corp) was installed to control the microscope. Exposure time was set to 20 ms. Framerate was set to either 2 Hz or 21 Hz. Scavenger buffer for SMT measurements had additional 2 mM UV-treated trolox, 10 mM 2-Mercaptoethanol (BME), 20 mM glucose, 320 μg/mL glucose oxidase, 50 μg/mL catalase and 0.1 mg/mL Bovine Serum Albumin (BSA) in working buffer (5). All analysis were performed on the central 350 by 350 pixel region of the images to minimize uneven illumination. Single-molecule images were analyzed with customized program written in Igor Pro ver. 6.22A (1). The positions and times of LAT trajectories were saved for time-averaging MSD analysis (6): $MSD(n\delta t) = \frac{1}{N-n-1}\sum_{j=1}^{N-n-1}\{[x(j\delta t + n\delta t) - x(j\delta t)]^2 + [y(j\delta t + n\delta t) - y(j\delta t)]^2\}$, where δt is the time between frames, N is the total number of frames in a single trajectory, and n and j are positive integers. The MSD analysis evaluates one trajectory at a time; inspecting many trajectories then provides statistics for various parameters of LAT subdiffusion, such as the characteristic timescales.

Bayesian change-point analysis

The detail derivation of the algorithm is shown in the work by Ensign and Pande (7). In brief, the algorithm evaluates a Bayes factor from a trajectory to describe the likelihood that a change point occurs relative to the likelihood that no change takes place:

$$\text{Bayes Factor} = \frac{P(D|H_2)}{P(D|H_1)} = \frac{|\langle x\rangle|}{2^{\frac{1}{2}}\pi^{\frac{3}{2}}(Ns^2)^{-\frac{N}{2}+\frac{1}{2}}\Gamma(\frac{N}{2}-1)}\left\langle\frac{\prod_{\alpha=1,2}N_\alpha^{-\frac{N_\alpha}{2}+\frac{1}{2}}(s_\alpha^2)^{-\frac{N_\alpha}{2}+1}\Gamma(\frac{N_\alpha}{2}-1)}{(s_1^2+s_2^2)(\langle x_1\rangle^2+\langle x_2\rangle^2)}\right\rangle$$

where D is data, H_1 is no change in the trajectory, H_2 is at least one change in the trajectory, N is the number of data points, s is the standard deviation, the subscripts denotes segment by a changepoint (say t_s is the hypothetic change point, then N_1 is the number of data points prior to t_s and N_2 is the number of data point after t_s), and $\langle\cdot\rangle$ denotes averaging over all possible change-point positions (in the case of Gaussian statistics considered here, it is averaged over $N-5$ values since standard deviation requires at least 3 observables to converge). We chose a threshold Bayes factor of 3 for substantial evidence of a transition occurring within the trajectory if the calculated Bayes factor exceed this value. However, since the degree of freedom in our implementation is the derivative of MSD, it will amplify noise such that the existence of a

change point can be underestimated. Therefore, Bayes factor is just a guideline in this application. The more important application of the algorithm is the estimation of where the transition takes place, based on the posterior distribution of change point positions:

$$P(t_s|D,H_2) \propto \frac{\prod_{\alpha=1,2} N_\alpha^{-\frac{N_\alpha}{2}+\frac{1}{2}} (s_\alpha^2)^{-\frac{N_\alpha}{2}+1} \Gamma(\frac{N_\alpha}{2}-1)}{(s_1^2+s_2^2)(\langle x_1\rangle^2\langle x_2\rangle^2)}$$

The peak of the distribution is where the change point is most likely to occur. The equations used in our analysis are from the Eq. [35] and Eq. [37] of the original work. This analysis can be applied multiple time for multi-change-point detections. After detecting the first (and the most probable) change point, the trajectory is segmented into two fragments by the first change point. We then apply the same algorithm to each of the two fragments for detection of the second change point. This can be repeated multiple time, but in our application, we use it at most twice to evaluate the reptation time and the Rouse time in the LAT trajectories.

Comparison of LAT data with the reptation model

Parameters are calculated by comparing characteristic timescale from single-molecule data of LAT with the reptation model (Fig. 4B). The assignment of the observed timescales to the model is established by recognizing that each scaling follows a particular order ($\tau_{rep} > \tau_R > \tau_e$) with the reptation time τ_{rep} transition from subdiffusive to diffusive motion, i.e. the slowest characteristic timescale in Fig. 2 will correspond to τ_{rep}. Next, this mapping, along with relations in the reptation model gives the following equations (Fig. 4B):

Reptation time $\tau_{rep} = 6\tau_0 N_e^2 \left(\frac{N}{N_e}\right)^3 = 5.1\ s$ Eq. [1]

Rouse time $\tau_R = \tau_0 N^2 = 0.64\ s$ Eq. [2]

Rouse time of entangled strand $\tau_e = \tau_0 N_e^2$=not observed due to resolution limit(~100ms) Eq. [3]

where N_e is number of monomers in an entangled strand, N is the total number of monomers in the polymer, τ_0 is the monomer relaxation time. Although these equations cannot solve for all variables, we can calculate the ratio of N/N_e and τ_e. By dividing Eq. [1] by Eq. [2], $N/N_e \sim 1.3$. Inserting this result back to Eq. [1] gives $\tau_e \sim 300$ ms.

Monte Carlo simulations

The main purpose of the simulations is to show that different subdiffusion mechanism may be distinguishable from experimental MSD analyses. For this purpose, we consider the simplest case for each mechanism. All simulations initiate with a particle in infinite 2D squared lattices. In each step of random walk simulation, the particle randomly moved along one axis of the lattices. The positions and times of each step were saved and analyzed following the same MSD analysis in the experiments. Since the goal is to inspect the qualitative shape of MSD for each mechanism, most parameters are arbitrary chosen such that the shape of MSD are resolved within the simulation time. All simulations were performed in Matlab R2016a.

Polymer constraints

The algorithm for simulating subdiffusion of a polymer largely follows Verdier-Stockmayer model (8-10). The tagged molecules belongs to a polymer of $N = 20$ beads (we chose an intermediate size polymer since a larger size requires longer simulation time and a short polymer has subdiffusion only at a very fast timescale). We consider the simpliest case of polymer

network since the structural orientation of LAT is unknown (an intrinsically disordered protein) – a non self-avoiding polymer on a 2D lattices by itself. The network is initiated by randomly orienting the polymer bonds on a 2D lattices. Occasionly, this leads to an immobile network, which we discard. Then, the polymer moves according to the rules described in Verdier-Stockmayer model. During each time unit of $1/N$, a random monomer in the network is chosen to move. The local bond geometry of the tagged paricle is examined to determine legal movements. There are three types of allowed motions: ***i)*** if the two adjacent bonds connecting the particle are perpendicular to each other, the particle then moves to opposite corner such that both of the bonds are flipped by 90 degree – referred to as "coner move", ***ii)*** if the two adjacent bonds are overlapping each other, the particle will randomly redirect both of the bonds – referred to as "kink jump", and, ***iii)*** if the bead at either end point, it reorient the single bonds randomly. Any other type of motions were restricted by bond constraints in the simulations. A schematic for the described allowed motions are shown in p. 391 in Rubinstein and Colby, *Polymer Physics* (10).

Confinement

The particle follows standard random walk described earlier, except that the 2D lattices are confined in a 20 by 20 unit impassable square box (the length of the confinement is chosen to result in a similar timescale to polymer constraints). If the particle randomly attempt to cross the boundary, it will remain at the same spot. This exemplify the case of picket-and-fence model commonly discussed in the plasma membrane.

Crowding effect

We consider the case of crowding in a dynamic environment using continuous time random walk, following the work by Condamin (11). After the tagged particle moving to a new position, the molecule is trapped with a waiting time following a heavy-tail probability distribution (11, 12): $P(1 < T < t) = 1 - t^{-\alpha}$, and $P(T < 1) = 0$. α was chosen to be 0.5.

Bond dynamics

The effect of pure bond dynamics is considered by having the tagged particle randomly binding to immobile sites on 2D lattices (Fig. 3D). Each time the particle move to a new position, we set a probability of 0.2 to become engaged in an immobile site for a 200-unit lifetime (chosen to compare with the characteristic timescale of polymer motion). This represent the case where the molecular motions from binding-and-rebinding greatly exceed that of local movement of the network. Binding to a mobile polymer network (Fig. 3E) is evaluated similarly except that the bond lifetime is 50 or 500 unit (depending on whether we are looking at short or long bond lifetime). During the bond lifetime, the particle resumes the motion as described in polymer constraints.

Reference

1. Huang, W. Y. C., Q. Yan, W. C. Lin, J. Chung, S. D. Hansen, S. M. Christensen, H. L. Tu, J. Kuriyan, and J. T. Groves. 2016. Phosphotyrosine-mediated LAT assembly on membranes drives kinetic bifurcation in recruitment dynamics of the Ras activator SOS. Proc. Natl. Acad. Sci. USA 113:8218-8223.
2. Yan, Q., T. Barros, P. R. Visperas, S. Deindl, T. A. Kadlecek, A. Weiss, and J. Kuriyan. 2013. Structural basis for activation of ZAP-70 by phosphorylation of the SH2-kinase linker. Mol. Cell. Biol. 33:2188-2201.
3. Nye, J. A., and J. T. Groves. 2008. Kinetic control of histidine-tagged protein surface density on supported lipid bilayers. Langmuir 24:4145-4149.
4. Lin, W. C., L. Iversen, H. L. Tu, C. Rhodes, S. M. Christensen, J. S. Iwig, S. D. Hansen, W. Y. C. Huang, and J. T. Groves. 2014. H-Ras forms dimers on membrane surfaces via a protein-protein interface. Proc. Natl. Acad. Sci. USA 111:2996-3001.
5. Cordes, T., J. Vogelsang, and P. Tinnefeld. 2009. On the Mechanism of Trolox as Antiblinking and Antibleaching Reagent. J. Am. Chem. Soc. 131:5018-5019.
6. Rozovsky, S., M. B. Forstner, H. Sondermann, and J. T. Groves. 2012. Single Molecule Kinetics of ENTH Binding to Lipid Membranes. J. Phys. Chem. B 116:5122-5131.
7. Ensign, D. L., and V. S. Pande. 2010. Bayesian Detection of Intensity Changes in Single Molecule and Molecular Dynamics Trajectories. J. Phys. Chem. B 114:280-292.
8. Verdier, P. H., and W. H. Stockmayer. 1962. Monte Carlo Calculations on Dynamics of Polymers in Dilute Solution. J. Chem. Phys. 36:227-+.
9. Baumgartner, A. 1984. Simulation of Polymer Motion. Annu. Rev. Phys. Chem. 35:419-435.
10. Rubinstein, M., and R. H. Colby. 2003. Polymer Physics. Oxford University Press, New York, U.S.A.
11. Condamin, S., V. Tejedor, R. Voituriez, O. Benichou, and J. Klafter. 2008. Probing microscopic origins of confined subdiffusion by first-passage observables. Proc. Natl. Acad. Sci. USA 105:5675-5680.
12. Izeddin, I., V. Recamier, L. Bosanac, I. I. Cisse, L. Boudarene, C. Dugast-Darzacq, F. Proux, O. Benichou, R. Voituriez, O. Bensaude, M. Dahan, and X. Darzacq. 2014. Single-molecule tracking in live cells reveals distinct target-search strategies of transcription factors in the nucleus. eLife 3:e02230.

Supporting Figures

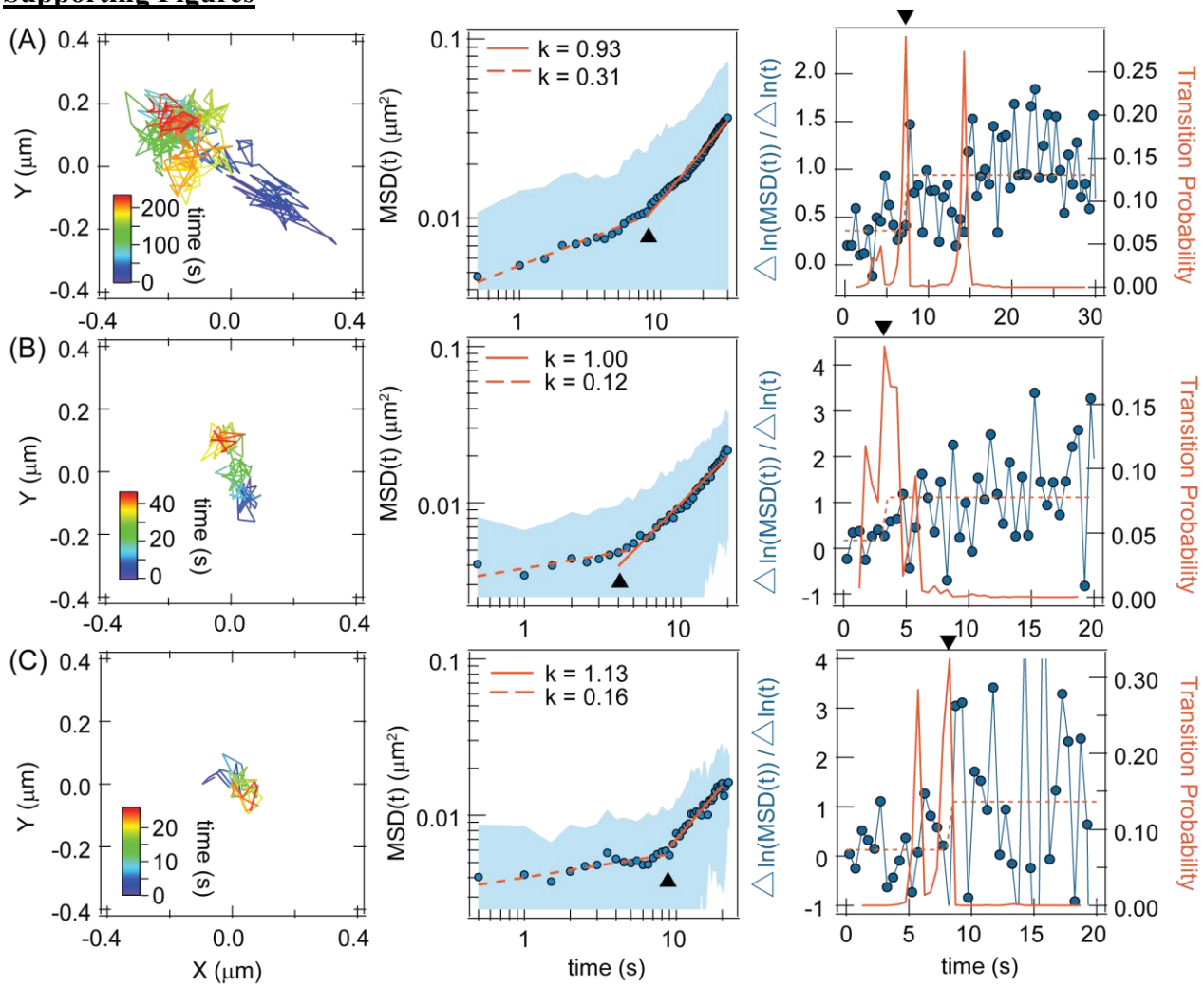

FIGURE S1. Additional examples of LAT subdiffusion. Single-molecule tracking of dilute labeled LAT within assemblies, time-averaging MSD analysis, and Bayesian change-point analysis are shown in the left, middle, and right column, respectively. The time axis is color coded in the trajectory. Time-averaging MSD plots are fitted to a power law in log-log plot. Shaded area is the standard deviation of statistics from a single trajectory. The fitted $\{A_{k\sim1}, A_{k<1}\}$ for top, middle, and bottom MSD are {0.0015, 0.0054}, {0.00098, 0.0039}, and {0.00052, 0.0040}, respectively.

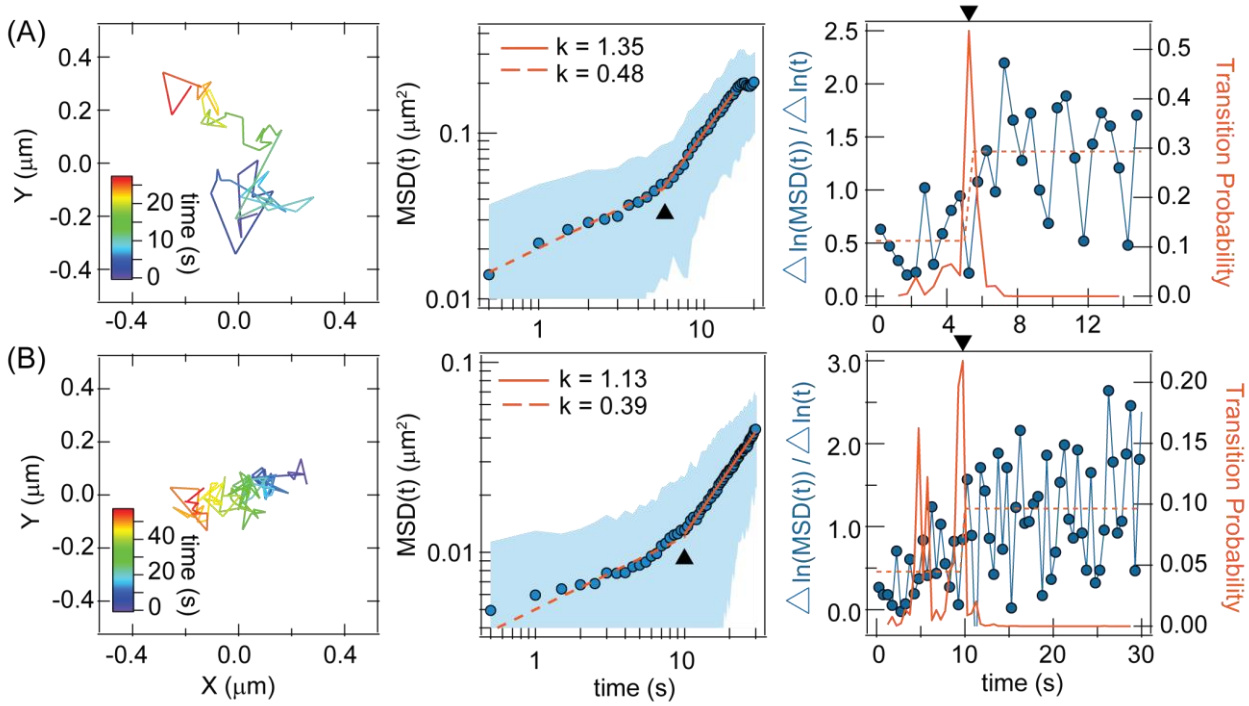

FIGURE S2. Time-dependent subdiffusion of Grb2 and SOS. Representative examples of Grb2 (top) and SOS (bottom) trajectory analysis within assembly structure. The long dwell times of Grb2 and SOS reflect their multivalent interactions with the assemblies (1). The time axis is color coded in the trajectory. Time-averaging MSD plots are fitted to a power law in log-log plot. Shaded area is the standard deviation of statistics from a single trajectory. The fitted $\{A_{k\sim1}, A_{k<1}\}$ for Grb2 and SOS are {0.0045, 0.020} and {0.00090, 0.0050}, respectively.

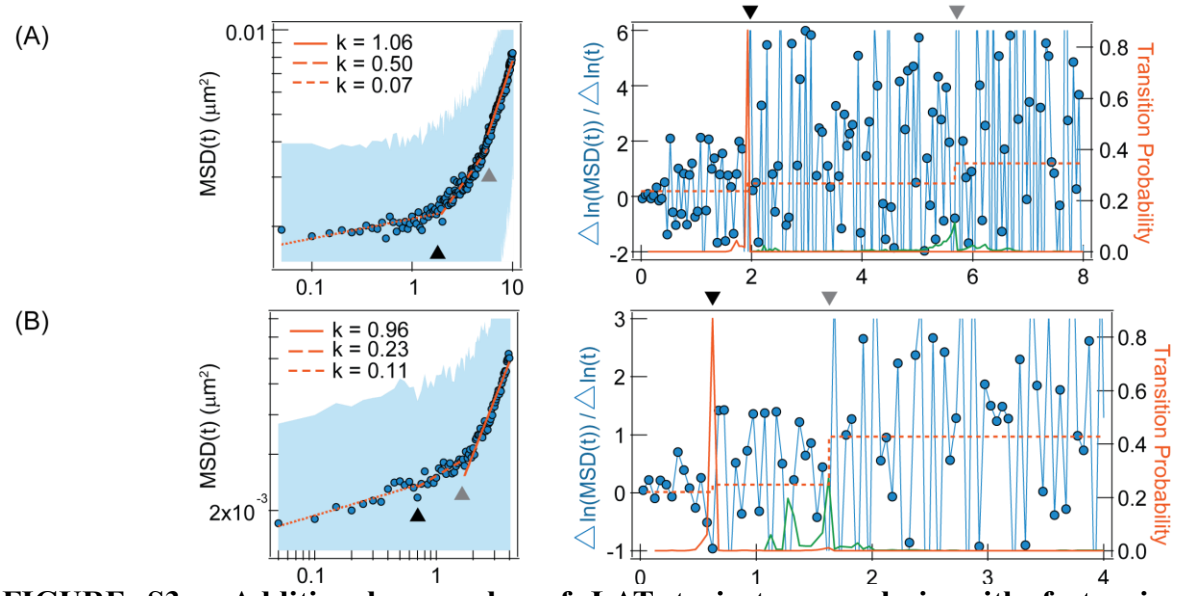

FIGURE S3. Additional examples of LAT trajectory analysis with faster imaging acquisition. MSD analysis of LAT mobility acquired at a framerate of 21 Hz. Shaded area is the standard deviation of statistics from a single trajectory. Each timescale is fitted by a power law, with the characteristic timescales denoted by triangles. The fitted A for $k = 1.06,0.50,0.07,0.96,0.23,0.11$ are 0.00067, 0.0015, 0.002, 0.0016, 0.0027, and 0.0025, respectively. The orange and green curve of the right plot corresponds to the transition probability calculated from the full timescale and the partial timescale after to the faster (black triangle) characteristic timescale, respectively.

Supporting Movie

Movie S1. Single-molecule imaging of LAT. Imaging of LAT-Alexa Flour 555 at a frame rate of 2 Hz. Most of the particles are mobile over longer timescales (>10 s).